Chapter 1

Super-Resolution Imaging of Mitotic Spindle Microtubules Using STED Microscopy

Isabella Koprivec, Valentina Štimac, and Iva M. Tolić

Abstract

Stimulated emission depletion (STED) microscopy is a powerful super-resolution imaging technique that only recently entered the field of mitosis, where it proved to be invaluable for studying various microtubule classes, kinetochore-microtubule attachments and chromosome segregation errors. Here, we describe immunofluorescence combined with STED microscopy as a method for analyzing microtubules and kinetochore-microtubule attachments in human mitotic spindles. We also describe live-cell STED microscopy as a method for single-plane short-term imaging of transient processes in crowded spindle areas. Finally, we outline image analysis approaches for the quantitative assessment of microtubule bundles within the spindle.

Key words STED microscopy, Cell division, Mitosis, Mitotic spindle, Microtubules, Kinetochores, Chromosomes, Nucleation, Attachments, Segregation errors

1 Introduction

Stimulated emission depletion (STED) microscopy is a super-resolution microscopy technique first introduced in 1994 [1, 2]. STED microscopy overcomes the diffraction limit of confocal microscopy by using a doughnut-shaped depletion laser to deplete the emitted fluorescence at specific positions, thus limiting emission only to the central "zero"-intensity laser spot [3]. Since STED can reach a resolution of up to 20 nm [4], it has been widely used to image structures and distribution of proteins within the cell. The power and versatility of STED microscopy are particularly evident in neuroscience, where visualization of cytoskeletal filaments and synaptic compartments has shed light on the architecture and motility of neurons, functions of synapses, dynamics of signal transmission, and neuron-glial interactions [5]. Moreover, STED microscopy

Authors Isabella Koprivec and Valentina Štimac have contributed equally to this chapter.

Tomomi Kiyomitsu (ed.), *The Mitotic Spindle: Methods and Protocols*, Methods in Molecular Biology, vol. 2872,
https://doi.org/10.1007/978-1-0716-4224-5_1,

proved invaluable for our understanding of complex organelles, as it elucidated the nanoscale distribution of mitochondrial proteins [6, 7] and cristae dynamics in mitochondria [8]. In mitosis, various super-resolution microscopy techniques have been used to resolve the centrosome [9] and the kinetochore [10] structure. Yet the visualization of fine or densely arranged microtubules within the spindle remained one of the biggest challenges. Luckily, the advent of STED microscopy in mitosis over the past few years enabled us to understand the complex landscape of spindle microtubules, their mutual interactions and the various attachments they form with kinetochores on chromosomes. The technique has since been used for studying mitosis in the malaria parasite (*Plasmodium berghei*), Indian Muntjac fibroblasts and various human cell lines, and even made its way to the clinic as part of the safety evaluation for limbal stem cells used in eye regeneration [11–19]. With its varied applications, STED has helped answer many of the long-standing questions about the shapes of microtubule bundles within the metaphase spindle [12], midzone microtubules during anaphase [13], early spindle formation [14], spindle microtubule growth [15], and previously indistinguishable microtubule classes and chromosome segregation errors [16].

Here, we compare STED microscopy to existing approaches (*see* **Note 1**) for studying spindle microtubules and discuss the advantages and disadvantages of STED microscopy (*see* **Note 2**). We also provide detailed protocols for immunostaining and live-cell STED super-resolution imaging of microtubules within human spindles, together with the accompanying image analysis approaches.

2 Materials

2.1 Cell Culture and Immunostaining

1. hTERT-RPE1 cells stably expressing either CENP-A-GPF or both CENP-A-GFP and Centrin1-GFP (*see* **Note 3**).
2. Cell culture medium: Dulbecco's Modified Eagle's Medium with 1 g/L D-glucose, pyruvate and L-glutamine (DMEM), supplemented with 10% (vol/vol) heat-inactivated Fetal Bovine Serum (FBS) and penicillin (100 IU/mL)/streptomycin (100 mg/mL) solution.
3. 35 mm uncoated glass coverslip dishes with 0.17 mm glass thickness (MatTek Corporation or Ibidi GmbH).
4. Cytoskeleton extraction buffer (CEB): 0.5% w/v Triton-X-100, 0.1 M PIPES, 1 mM EDTA and 1 mM $MgCl_2$ in milli-Q water. We use UltraPure 0.5 M EDTA (pH = 8.0, 15575020, Invitrogen). We recommend first preparing 5% w/v Triton-X-100, 1 M PIPES solution (pH = 7.0), and 1 M $MgCl_2$ solutions and diluting them in milli-Q water.

Store CEB for a maximum of three weeks at room temperature to achieve the best results. Before use, aliquot CEB into smaller volumes and pre-warm the aliquot to 37 °C to prevent mitotic spindle shrinkage at temperatures lower than 37 °C (*see* **Notes 4** and **5**).

5. Fixation solution: 3% paraformaldehyde and 0.1% glutaraldehyde solution in PBS. Add 3 mL of 4% paraformaldehyde, 8 μL of 50% glutaraldehyde, 0.4 mL 10× PBS and fill up with milli-Q water until 4 mL. The fixation solution should be made fresh each time and pre-warmed to 37 °C to prevent mitotic spindle shrinkage at temperatures lower than 37 °C.
6. Reduction buffer: 0.1% w/v sodium borohydride solution. Dissolve 10 mg of sodium borohydride in 10 mL of 1× PBS (hydrogen gas bubbles should appear upon dissolving). Make a fresh solution each time and handle sodium borohydride with care as it is reactive.
7. Quenching buffer: 100 mM glycine in 1× PBS. The solution can be stored for several months at 4 °C.
8. Blocking/permeabilization (B/P) buffer: 1% w/v NGS and 0.5 w/v Triton-X-100 in milli-Q water. The B/P buffer can be stored for several months at −20 °C.
9. Antibodies: Rat monoclonal tubulin (diluted 1:500, MA1-80017, Invitrogen), donkey anti-rat Alexa Fluor 568 or 594 (diluted 1:100, ab175475 and ab150156, Abcam); *see* **Note 6** and Table 1 for tips on how to choose the right antibody.

2.2 STED Imaging

1. STED microscope: our STED images are acquired on the Expert Line easy3D STED microscope system (Abberior Instruments), equipped with a pulsed STED laser at 775 nm (*see* **Note 7**).

Table 1
Choosing the right secondary antibody.

Alexa Fluor 594	Alexa Fluor 647	STAR RED
Very resistant to photobleaching	Very sensitive to photobleaching	Medium sensitivity to photobleaching
Enables imaging of the entire z-stack	Usually enables imaging of only 1–3 z-planes	Usually enables imaging of 3–10 z-planes
Each cell can be imaged multiple times	A cell can be imaged only once	A cell can be imaged only once
Requires high STED laser power to achieve an appropriate resolution	Requires less STED laser power to achieve the appropriate resolution	Requires very little STED laser power to achieve the appropriate resolution

2. Sample with beads: we use the Abberior nanoparticle alignment slide (*see* **Note 8**).
3. 100×/1.4NA UPLSAPO100× oil objective (Olympus).
4. 60×/1.2NA UPLSAPO60× water objective (Olympus).
5. Immersion oil and lens cleaning tissues: Immersion oil type F30CC (stable at 23 °C) and type 37LDF (stable at 37 °C); Whatman lens cleaning tissue Grade 105 (*see* **Note 9**).
6. Tubulin and DNA dyes: SiR-tubulin kit (contains 50 nmol SiR-tubulin and 1 μmol verapamil, Spirochrome) for live-cell imaging; SPY-DNA dye series (Spirochrome) for live-cell imaging and DAPI for immunofluorescence (*see* **Note 10**).
7. Incubator chamber that controls the temperature at 37 °C and CO_2 at 5% for live cell imaging.
8. Software: Imspector software or Fiji/ImageJ.

3 Methods

3.1 Cell Culture and Immunostaining

For immunostaining, we optimized the first steps and chemicals of two previously published protocols for expansion microscopy [20, 21]. We used a fixation solution containing glutaraldehyde, which was demonstrated to be the best option for visualizing microtubules in the mitotic spindle [20]. For experiments described in this article, we used hTERT-RPE1 cells stably expressing either CENP-A-GPF or both CENP-A-GFP and Centrin1-GFP. All protocols are optimized for these cell lines.

1. Plate the cells 1–2 days before the fixation and keep them at 37 °C and 5% CO_2. The optimal confluency of cells on the day of fixation should be 80–90%, corresponding to the highest number of mitotic cells. We use 35 mm uncoated glass coverslip dishes with 0.17 mm glass thickness and seed the cells in 1 mL of the appropriate cell medium.
2. Remove the cell media from the dishes and add 500–1000 μL of pre-warmed CEB for 15 s to permeabilize cells and remove the cytoplasmic components that would otherwise result in unspecific binding of antibodies. CEB must be removed after 15 s because further exposure will cause the mitotic cells to detach, as CEB largely disrupts the membrane (*see* **Notes 5** and **6**).
3. Immediately after removing CEB, add 1 mL of pre-warmed fixation solution to the dish and incubate for 10 min at room temperature.
4. Aspirate the fixation solution and add 1 mL of the reduction solution for 7 min at room temperature. Sodium borohydride reduces the autofluorescence of glutaraldehyde from the fixation solution.

5. Aspirate the reduction solution and add 1 mL of the quenching solution for 10 min at room temperature. Glycine binds aldehyde groups from the fixation solution and reduces the unspecific binding of antibodies.
6. Remove the quenching solution and incubate the cells with 1 mL of B/P buffer for 2.5 h at 4 °C on the orbital shaker. This further permeabilizes the cells and prevents the unspecific binding of antibodies.
7. Incubate the sample with 300 µL of the primary antibody diluted in B/P buffer overnight at 4 °C on the orbital shaker. We achieved the best results using the rat monoclonal tubulin at 1:500 dilution.
8. The following day, wash the sample 3×, for 5 min each time, with 1 mL of 1× PBS at room temperature on the orbital shaker.
9. Incubate the sample with 300 µL of the secondary antibody diluted in B/P buffer for 1 h at room temperature on the orbital shaker. We use Alexa Fluor 568 or 594 antibodies at 1:1000 dilution (*see* **Note 7**).
10. Wash the sample 3×, for 5 min each time, with 1 mL of 1× PBS at room temperature on the orbital shaker.
11. Additionally, chromosomes can be stained using 1 mL of DAPI solution (1 µg/mL) for 10 min at room temperature on the orbital shaker.
12. Wash the DAPI solution 3×, for 5 min each time, with 1 mL of 1× PBS. Store the sample in 1 mL of 1× PBS at 4 °C for a maximum of three weeks. The fluorescence signal is the best when imaging is performed immediately after immunostaining.

3.2 Staining Tubulin with a Live-Cell Dye

1. Seed the cells 1–2 days before live-cell imaging on 35 mm uncoated glass coverslip dishes with 0.17 mm glass thickness in 1 mL of the appropriate medium and keep them at 37 °C and 5% CO_2. The optimal confluency of cells on the imaging day should be 80–90%, corresponding to the highest number of mitotic cells.
2. Dissolve the contents of SiR-tubulin kit vials according to the manufacturer's instructions. Add 50 µL of fresh anhydrous DMSO to the SiR-tubulin vial to make a stock concentration of 1 mM. Dissolve verapamil in 100 µL of fresh anhydrous DMSO to make a stock concentration of 10 mM (1000×).
3. Take 1 mL of cell medium from the dish with cells and add 0.1 µL of the SiR-tubulin dye to this 1 mL medium to make a final dye concentration of 100 nM. To avoid dye efflux, add 1 µL of the efflux pump inhibitor verapamil along with the dye

to 1 mL of cell medium. Resuspend the staining solution well and add it to the cells (if there is any remaining medium on the cells, remove it before adding the staining solution). Utilizing the old cell medium is essential because the fresh one can stop the cells from dividing.

4. Incubate for 1 h at 37 °C and 5% CO_2 before imaging.

3.3 STED Imaging of Fixed Samples

1. Before imaging, turn on the microscope system (use manufacturer's recommendations depending on the system) and put the dishes with fixed samples at room temperature for at least 30 min before the session. This ensures that the temperature of the sample is equilibrated to room temperature, preventing the sample drift during imaging.
2. Ensure the system is properly aligned using the sample with beads and follow the manufacturer's instructions for automatic and manual alignment.
3. For fixed sample imaging, choose the 100× objective and put a drop of immersion oil on the lenses. Put the dish with the sample on the stage and find focus using the brightfield or epifluorescence. Be aware that the epifluorescence can cause photobleaching before imaging, so use it only when necessary.
4. Find mitotic cells using eyepieces (for example, use the DAPI signal to discern mitotic phases based on the appearance of DNA).
5. Set up the protocol for STED imaging. Determine the size of the region of interest (ROI) to encompass the entire cell. Set the pixel size to 20 nm. The Expert Line easy3D STED microscope system can go down to 10 nm, but you should remember that lowering pixel size significantly increases the imaging time. Therefore, the pixel size should be adjusted to meet the requirements regarding the final image resolution and imaging duration.
6. Select either 2D or 3D STED based on whether you need better lateral (XY) or axial (Z) resolution, respectively. Since we usually require the best possible resolution between microtubules in the spindle midzone in the XY plane, we use 2D STED (*see* **Note 11**).
7. Determine the laser powers for each wavelength and the 775 nm STED line based on the photobleaching of your sample. We use the 488 nm laser to excite CENP-A-GFP (40% laser power) and the 561 nm laser to excite Alexa Fluor 594 (20% laser power). To achieve proper super-resolution of microtubules (*see* Subheading 3.6), the 775 nm STED laser for depleting the red line was set to 45%.

8. Additionally, adjusting dwell time (for how long the laser is applied to the sample) and line accumulation (the number of scans) is critical to achieve the best resolution. Keep in mind that increasing these two settings also increases the imaging time and photobleaching of the sample. We got the best results when we adjusted the dwell time to 10 μs and the line accumulation to 1. The pinhole size determines the amount of out-of-focus light reaching the detector. A better resolution is achieved when the pinhole size is smaller. For our purposes, we set the pinhole size to 1.0 AU. The described settings result in an average of 100–200 photons collected at the avalanche photodetector for each channel, corresponding to the optimum signal collection and the best resolution.
9. Before imaging, adjust the Z-stack's first and last planes and the distance between the planes. Alternatively, you can determine the middle plane of your image and set the total distance you want to acquire. *See* Table 1 for more information on fluorophore stability.
10. After the acquisition, shut down the system and clean the objective lenses with Whatman lens cleaning tissue.

3.4 Live-Cell STED Imaging

We imaged microtubules stained with 100 nM SiR-tubulin in an RPE1 cell line that stably expresses CENP-A-GFP and Centrin1-GFP and the following protocol was specifically adapted for this cell line. Imaging with SiR-tubulin dye at this concentration can be performed only for 45–60 min because the high concentration of the dye results in microtubule stabilization and the accompanying toxic effects after that point.

1. Heat the incubator chamber to 37 °C for live-cell imaging and adjust CO_2 to 5% after turning on the system. The cells must be kept in controlled conditions to ensure cell health.
2. Use either 100× oil objective or 60× water objective (*see* **Note 9** for tips on choosing the right objective). Use the appropriate immersion for the objective (if you decide to use the oil objective, we recommend an oil that is stable at 37 °C to avoid the drift of the sample). Focus the sample using the brightfield optics and find mitotic cells based on the CENP-A signal. Alternatively, SPY-DNA dyes at 20–40 nM concentration can be used for cell lines that do not express fluorescent proteins.
3. Follow **steps 5**–**9** from the protocol for *STED imaging of fixed samples*. ROI can include only a small part of the spindle (e.g., astral region or midzone) to reduce the photobleaching and expedite the imaging. We used the following laser powers for our sample: 488 nm to 15%, 640 nm to 30%, and the 775 nm STED laser to 10%. Pixel size was set to 25 nm, dwell time to 7 μs, line accumulation to 5, pinhole size to 1.0 AU and STED mode to 2D.

4. We used a single z-plane for the imaging of microtubules in the whole spindle because imaging is slow (~45 s per plane). In cases where you want to image a small ROI, the number of z-planes can be increased based on the dynamics of the process you want to image. If you wish to image cells during certain time periods, adjust the total time of imaging and the time interval between frames while also checking for signs of phototoxicity (e.g., spindle shrinkage).
5. After the acquisition, shut down the system and clean the objective lenses with Whatman lens cleaning tissue.

3.5 Using STED Microscopy for the Detection of Individual Microtubules in Crowded Environments

Compared to confocal microscopy, STED microscopy enables precise visual detection of various microtubule bundles within the spindle. In addition to providing stunning images of mitotic spindles, it also allows for visual detection and analysis of microtubules in crowded areas, including the astral region and the spindle midzone (Fig. 1a–d). Where confocal microscopy detects only a faint signal indistinguishable from that of the background, STED microscopy captures even the very thin structures (Fig. 1b, d). Additionally, where confocal microscopy shows a single microtubule bundle, super-resolution can distinguish between two separate entities within the bundle (Fig. 1b, d). Thus, using STED microscopy to study microtubules within the mitotic spindle significantly increases the accuracy and precision of analysis.

3.6 Determining the Resolution

To determine the resolution of our STED microscopy protocol compared to confocal microscopy, we image the same spindle using confocal and STED microscopy protocols on the same microscope (Fig. 2a). We use the Line tool within the Imspector software or Fiji/ImageJ to draw a line perpendicular to an isolated astral microtubule and create an intensity profile (Fig. 2a). We then estimate the resolution as the width of the tubulin intensity peak at its half-maximum value, measured from the background value obtained using the 25 × 25 pixel Square Tool (Fig. 2b). We consider the protocol appropriate for imaging if the measured width is, on average, less than 90–100 nm. In the example in Fig. 2, the resolution of the STED image was estimated to be 66 nm, compared to 234 nm in the confocal image. This implies that STED imaging improved the spatial resolution by a factor of 3.5.

3.7 Using STED Microscopy to Study Microtubule Bundle Composition and Nucleation

STED microscopy, combined with image analysis, can be a powerful tool for quantitative analysis of microtubules within the spindle. Using a protocol we previously developed to measure the tubulin intensity of a specific microtubule bundle [12], we can determine the number of microtubules within a particular bundle at any time point and any position within the spindle. Provided that the microtubule bundle is relatively isolated from its neighbors, we place a

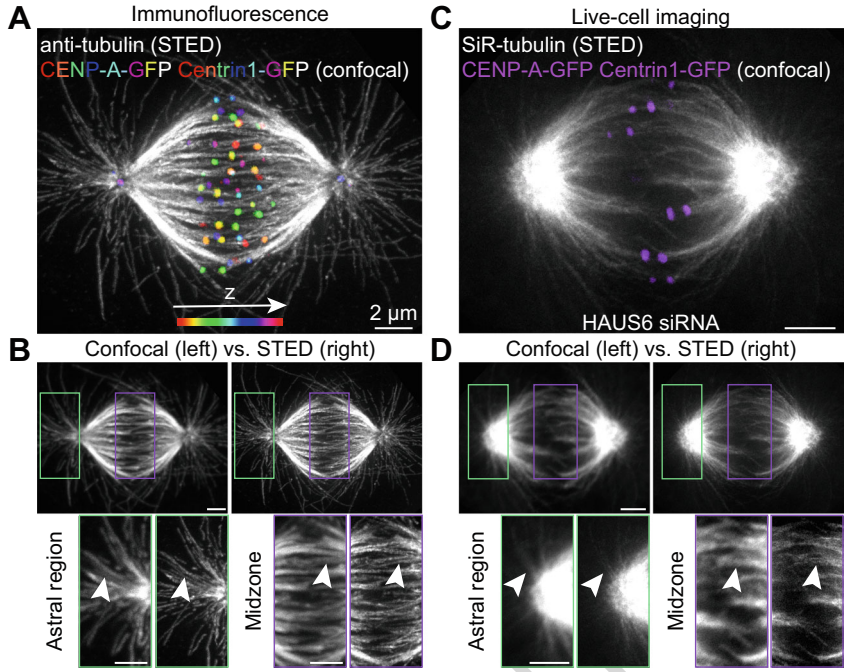

Fig. 1 STED microscopy for discerning individual microtubules. (**a**) STED super-resolution image of microtubules immunostained for α-tubulin (gray) in RPE1 cells stably expressing CENP-A-GFP and Centrin1-GFP (rainbow, confocal). The image shows a maximum intensity projection of 8 central z-planes of the metaphase spindle. Kinetochores and centrosomes are color-coded for depth with the Spectrum LUT in ImageJ throughout the 8 z-planes, corresponding to 2 µm. (**b**) Comparison of tubulin signal obtained using either confocal or STED microscopy to image the spindle from (**a**). Insets represent close-ups of the astral region and the spindle midzone. (**c**) STED super-resolution image of microtubules dyed with 100 nM SiR-tubulin (gray) in HAUS6-depleted RPE1 cells stably expressing CENP-A-GFP and Centrin1-GFP (purple, confocal). The image shows one central z-plane of the metaphase spindle. (**d**) Comparison of tubulin signal obtained using either confocal or STED microscopy to image the spindle from (**c**). Insets represent close-ups of the astral region and the spindle midzone. Arrowheads point to structures that could only be resolved using STED microscopy. The brightness and contrast were adjusted so that astral microtubules are similarly visible in all spindles in STED microscopy or that all captured microtubules are visible in insets. Scale bars, 2 µm

25 × 25 pixel Square tool in Fiji/ImageJ in the middle of the microtubule bundle of interest and then place another 25 × 25 pixel square in the empty nearby area to measure the background, on a single-plane image of the spindle (Fig. 3a). The microtubule bundle's intensity equals the bundle's measured intensity (mean intensity within the square) minus that of the background. To obtain the number of microtubules within the bundle of interest, we compare it against astral microtubules, which consist of single microtubules. To measure the tubulin intensity of astral microtubules, we again place one 25 × 25 pixel square on the astral microtubule and another in the empty nearby area to measure the background (Fig. 3a). Subsequently, we subtract the two values to obtain the final intensity of the astral microtubule. This can be

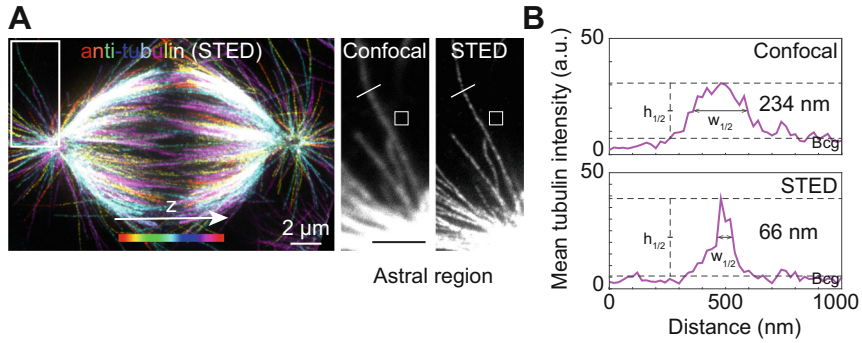

Fig. 2 Determining the spatial resolution. (**a**) STED super-resolution image of microtubules immunostained for α-tubulin (rainbow) in RPE1 cells stably expressing CENP-A-GFP (not shown). The image shows a maximum intensity projection of 6 central z-planes of the metaphase spindle. Microtubules are color-coded for depth with the Spectrum LUT in ImageJ throughout the 6 z-planes, corresponding to 1.8 μm. Insets represent sum intensity projections of the astral region obtained using either confocal or STED microscopy to image the spindle from (**a**). Line Tool (length = 1 μm, thickness = 1) and Square Tool (25 × 25 pixel, corresponding to 0.5 × 0.5 μm) from ImageJ are drawn on the insets and represent tools to measure the intensity profile of the astral microtubule and the mean intensity of the nearby background, respectively. (**b**) Intensity profiles of the 1 μm line drawn perpendicularly to the astral microtubule in ImageJ for astral microtubules imaged using either confocal or STED microscopy. Resolution is defined as the width of the peak at its half-maximum, after subtracting the background, and is considered appropriate when this value amounts to <100 nm. The brightness and contrast were adjusted so that astral microtubules are similarly visible in all spindles in STED microscopy or that all captured microtubules are visible in insets. Scale bars, 2 μm

repeated many times, and the average can be used to make a comparison. Finally, to calculate the number of microtubules, we divide the intensity of the microtubule bundle of interest by the intensity of the astral microtubule.

STED microscopy can also be used to study specific nucleation processes that can hardly be visible when using confocal microscopy, particularly kinetochore-mediated nucleation. When using centrinone, an inhibitor of polo-like kinase 4 (PLK4) [22], to remove one centrosome, we were able to directly visualize sites where microtubule nucleation at kinetochores took place - including small microtubule stubs that arose from the kinetochores and clusters that started forming from them to create the future pole of the acentrosomal spindle side (Fig. 3b).

3.8 Using STED Microscopy to Study Kinetochore-Microtubule Attachments and Chromosome Segregation Errors

In addition to studying microtubule nucleation, STED microscopy is a powerful method to study kinetochore-microtubule attachments and chromosome segregation errors. STED microscopy allows direct visualization of any type of attachment, including mature, early end-on and lateral attachments within the two poles, but also more complex attachments that peripheral kinetochores form before they reach the area between the two spindle poles (Fig. 4a). This is particularly useful since direct visualization of kinetochore-microtubule attachments can be combined with cell

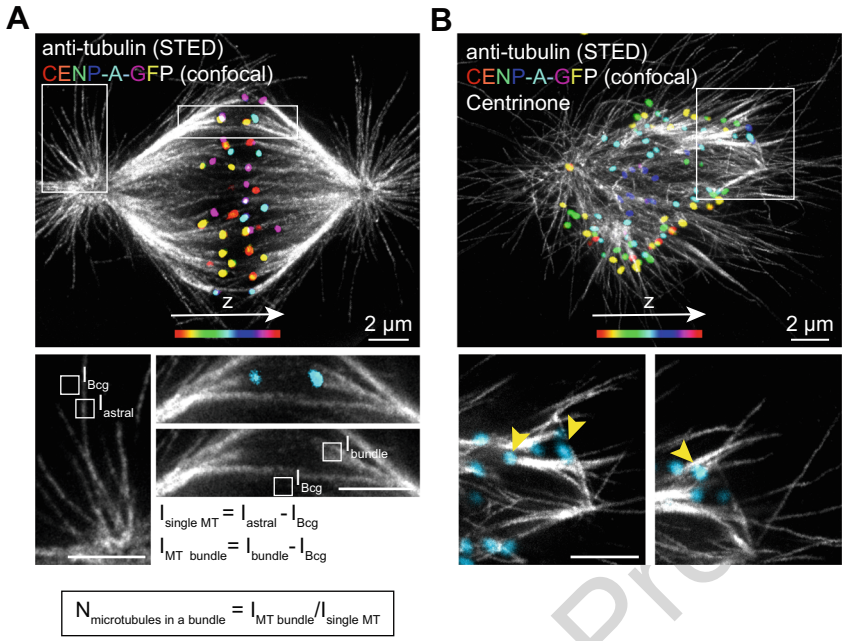

Fig. 3 Measuring the number of microtubules within a bundle and visualizing microtubule nucleation at the kinetochore. (**a**) STED super-resolution image of microtubules immunostained for α-tubulin (gray) in RPE1 cells stably expressing CENP-A-GFP (rainbow, confocal). The image shows a maximum intensity projection of 6 central z-planes of the metaphase spindle. Kinetochores are color-coded for depth with the Spectrum LUT in ImageJ throughout the 6 z-planes, corresponding to 1.8 µm. Insets show the astral region and the microtubules associated with one kinetochore pair from the spindle in (**a**). Square Tool (25 × 25 pixel) from ImageJ is drawn on the insets and represents a tool to measure the intensity of the astral microtubule, microtubule bundle of interest and the associated backgrounds, respectively. A formula to calculate the number of microtubules within the bundle of interest is provided below. (**b**) STED super-resolution image of microtubules immunostained for α-tubulin (gray) in RPE1 cells stably expressing CENP-A-GFP and Centrin1-GFP (rainbow, confocal) and treated with 300 nM centrinone to remove one centrosome. The image shows a maximum intensity projection of the entire prometaphase spindle. Kinetochores and centrosomes are color-coded for depth with the Spectrum LUT in ImageJ throughout 6 z-planes, corresponding to 1.8 µm. Insets show single z-planes of kinetochore-mediated microtubule nucleation sites, marked with yellow arrowheads. The brightness and contrast were adjusted so that astral microtubules are similarly visible in all spindles in STED microscopy or that all captured microtubules are visible in insets. Scale bars, 2 µm

lines that enable simultaneous analysis of stably expressed proteins, such as Mad2, a spindle assembly checkpoint protein that binds to kinetochores lacking mature end-on attachments [23], or the kinetochore protein Mis12 [24]. This combined approach can provide extensive information about the nature of the visualized attachments.

The ability of STED microscopy to precisely detect attachments of kinetochores, even with single microtubules, is revolutionary when it comes to studying chromosome segregation errors, especially merotelic attachments in which an individual kinetochore is bound to microtubules extending from the opposite poles

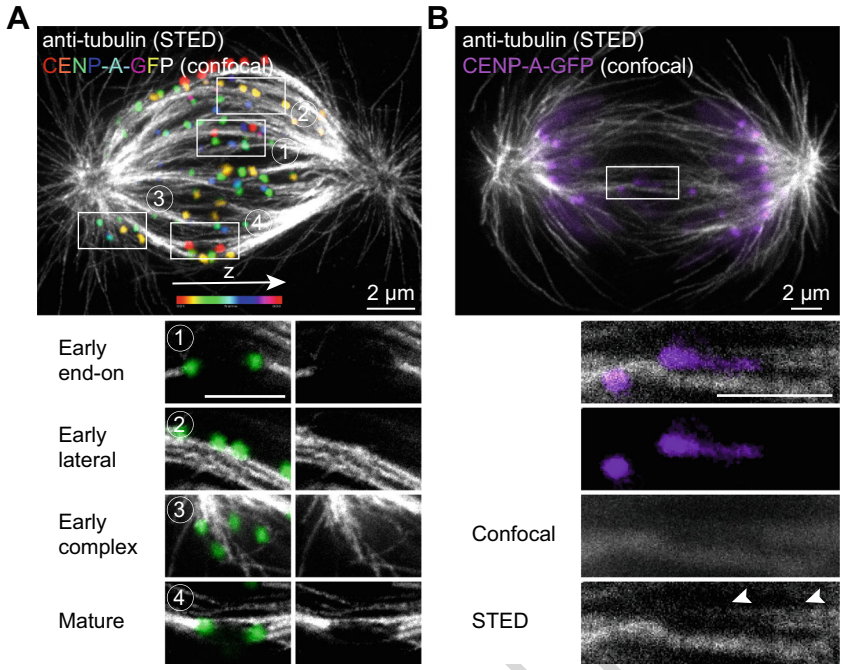

Fig. 4 Classifying kinetochore-microtubule attachments and identifying errors. (**a**) STED super-resolution image of microtubules immunostained for α-tubulin (gray) in RPE1 cells stably expressing CENP-A-GFP (rainbow, confocal). The image shows a maximum intensity projection of the entire prometaphase spindle. Kinetochores are color-coded for depth with the Spectrum LUT in ImageJ throughout 7 z-planes, corresponding to 2.1 µm. Insets show one z-plane or a maximum intensity projection of two z-planes with various types of attachments from the spindle in (**a**). (**b**) STED super-resolution image of microtubules immunostained for α-tubulin (gray) in RPE1 cells stably expressing CENP-A-GFP (purple, confocal) and treated with 200 µM CK-666 inhibitor of the Arp2/3 complex for 3 h. The image shows a single central z-plane. Insets represent close-ups of the merotelic attachment from the spindle in (**b**). Arrows point to the additional microtubule from the opposite side imaged using STED microscopy, which is undetectable when using confocal microscopy. The brightness and contrast were adjusted so that astral microtubules are similarly visible in all spindles in STED microscopy or that all captured microtubules are visible in insets. Scale bars, 2 µm

[25]. In addition to the previously used indicators of merotelic attachments, including stretching of the kinetochore and its central location on the anaphase spindle, several microtubules that form the erroneous attachment can now be directly visualized using STED microscopy, whereas they are undistinguishable from the background when using confocal microscopy (Fig. 4b). Not only that but STED microscopy can also be used to detect merotelic attachments even before they result in a lagging chromosome in anaphase while they are still located within a crowded metaphase plate [12].

4 Notes

1. Existing approaches for studying spindle microtubules and their attachments to chromosomes: Before STED, primary microscopy methods for detailed analysis of spindle microtubules were electron microscopy (EM) [26–30] or expansion microscopy (ExM) [20]. Even though EM is still a "gold standard" for studying spindles at a single-microtubule resolution, it is costly, time-consuming and unsuitable for live-cell imaging [31, 32]. Similarly, while much less expensive, ExM is also time-consuming and unsuitable for live-cell imaging. Thus, addressing numerous open scientific questions has relied on indirect approaches. For example, to study specific classes of microtubules within the spindle, several strategies have been developed: cold treatment was used to remove non-kinetochore microtubules and thus allowed the study of isolated kinetochore microtubules within the spindle [33]; a combination of hNuf2 and HSET RNAi was used to remove kinetochore microtubules and thus allowed the study of isolated non-kinetochore microtubules [34]; laser ablation was used to detect the connection between kinetochore microtubules and non-kinetochore microtubules that form a bridge between them, called bridging fibers [35]. Similarly, indirect approaches were employed to study kinetochore-microtubule attachments in healthy and error-prone cells: cold treatment was once again used to determine whether the kinetochore attaches to kinetochore microtubules or non-kinetochore ones [36, 37]; protein markers such as Mad1/2 or Bub1 were used to assess the stability of attachments [38, 39]; the interkinetochore distance, location in the central part of the spindle and stretching of the kinetochore were used as indicators of merotelic attachment [40, 41]. Yet, the arrival of STED microscopy to the cell division field allowed all of these phenomena to be visualized and studied more directly.
2. Advantages and disadvantages of STED microscopy: As with any method, there are several advantages and disadvantages to consider while determining whether STED microscopy is the right approach for a particular scientific question. Immunofluorescence combined with STED microscopy allows for a much shorter and simpler sample preparation protocol than electron microscopy and expansion microscopy—the entire sample preparation and imaging can be performed within three working days. Unlike the other two methods, STED also ensures that many cells are available for imaging in a dish or a slide, as the sample is minimally processed and rarely contains artifacts. In addition, STED can allow for user-friendly super-resolution

live-cell imaging with the SiR-tubulin dye [42], and it works well in combination with stably expressed proteins and tags [15]. Yet, the method is not without its limitations. Besides requiring a costly microscope system, it is important to carefully consider the choice of antibodies and dyes and to keep in mind that imaging the entire spindle can take up to several hours, which may be an issue if microscope availability is limited or large sample size is required. When using live-cell STED imaging, capturing the entire spindle is virtually impossible with the currently available systems, and one can only image a small region over a short period. With that in mind, STED microscopy remains a unique and powerful approach for studying spindle microtubules.

3. While we developed this protocol for RPE1 cells, it generally works as a good starting point for other cell lines in 2D and 3D cultures and for some organoids. However, further experimental optimization would likely be needed to achieve the appropriate resolution.
4. If the tubulin signal is weak or non-existent in the inner part of the spindle compared to the outer parts, in most cases, it means that the antibody did not penetrate the spindle. The problem might be that CEB is too old or some components have gone bad. We recommend preparing fresh ingredients and making an entirely new CEB.
5. If the spindles look shrunken or miss astral microtubules, the CEB and fixative were not properly pre-warmed. These two chemicals must be pre-warmed exactly to 37 °C.
6. To ensure you choose the appropriate secondary antibody, consult Table 1.
7. Be aware that the position of the system in the microscopy room is critical for obtaining the best super-resolution images. Avoid positioning the system close to the direct airflow from air conditioning or near any vibration. This will result in the drift of the sample or noise during imaging, respectively. (Note that vibrations can arise due to the music or mobile phone usage next to the system).
8. We recommend performing the system alignment before each session. Align all lasers in 2D and 3D and remember that the pinhole must be appropriately positioned to ensure the best results. Always check the beads after the automatic alignment procedure and do not simply rely on the precision of the automated protocol.
9. For the best possible super-resolution results, immersion and mounting media with the same refractive indexes should be used. While we found that the effect of this pairing is negligible

Table 2
Things to consider when using Taxol-based dyes for live-cell imaging

Advantages	Disadvantages
Allow for live-cell imaging	Need to be used in high concentrations (100–200 nM)
Strong signal	Short imaging window (1 h)
Fast penetration into cells	Unwanted effects on microtubule stabilization
Easy to use	Affinity for stable microtubules

when imaging spindles using the 2D STED mode, where PBS can be paired with an oil objective without a significant impact on the accuracy of the collected data, the effect can be much more significant when using 3D STED mode for imaging of very fine structures. As a general rule, we recommend using the 100×/1.4NA UPLSAPO100x oil objective for imaging mounted samples and the 60×/1.2NA UPLSAPO60x water objective for live-cell imaging.

10. For things to consider when using Taxol-based dyes for live-cell imaging, consult Table 2.
11. Choose 2D STED for primarily lateral (XY) super-resolution and 3D STED for axial (Z) super-resolution. Remember that switching from 2D to 3D STED increases the axial resolution but decreases lateral resolution and vice versa.

Acknowledgments

The authors thank Alexey Khodjakov for the RPE1 cell lines; Marko Šprem and the Abberior team for help with the Expert Line easy3D STED microscope system setup and developing microscopy protocols; all members of the Tolić group for helpful discussions and advice. The authors acknowledge funding by the European Research Council (ERC Synergy Grant, GA Number 855158), the Croatian Science Foundation (HRZZ) through Swiss-Croatian Bilateral Projects (project IPCH-2022-10-9344) and Cooperation Programme with Croatian Scientists in the Diaspora "Research Cooperability" (project PZS-2019-02-7653), and projects co-financed by the Croatian Government and the European Union through the European Regional Development Fund—the Competitiveness and Cohesion Operational Programme: IPSted (Grant KK.01.1.1.04.0057) and QuantiXLie Center of Excellence (Grant KK.01.1.1.01.0004).

References

1. Hell SW, Wichmann J (1994) Breaking the diffraction resolution limit by stimulated emission: stimulated emission-depletion fluorescence microscopy. Opt Lett 19:780–782. https://doi.org/10.1364/OL.19.000780
2. Klar TA, Hell SW (1999) Subdiffraction resolution in far-field fluorescence microscopy. Opt Lett 24:954–956. https://doi.org/10.1364/OL.24.000954
3. Vicidomini G, Bianchini P, Diaspro A (2018) STED super-resolved microscopy. Nat Methods 15:173–182. https://doi.org/10.1038/nmeth.4593
4. Göttfert F, Wurm CA, Mueller V et al (2013) Coaligned dual-channel STED nanoscopy and molecular diffusion analysis at 20 nm resolution. Biophys J 105:L01–L03. https://doi.org/10.1016/j.bpj.2013.05.029
5. Werner C, Sauer M, Geis C (2021) Super-resolving microscopy in neuroscience. Chem Rev 121(19):11971–12015. https://doi.org/10.1021/acs.chemrev.0c01174
6. Wurm CA, Neumann D, Lauterbach MA et al (2011) Nanoscale distribution of mitochondrial import receptor Tom20 is adjusted to cellular conditions and exhibits an inner-cellular gradient. PNAS 108(33):13546–13551. https://doi.org/10.1073/pnas.1107553108
7. Singh H, Lu R, Rodríguez PFG et al (2012) Visualization and quantification of cardiac mitochondrial protein clusters with STED microscopy. Mitochondrion 12(2):230–236. https://doi.org/10.1016/j.mito.2011.09.004
8. Stephan T, Roesch A, Riedel D et al (2019) Live-cell STED nanoscopy of mitochondrial cristae. Sci Rep 9:12419. https://doi.org/10.1038/s41598-019-48838-2
9. Mennella V, Keszthelyi B, McDonald KL et al (2012) Subdiffraction-resolution fluorescence microscopy reveals a domain of the centrosome critical for the pericentriolar material organization. Nat Cell Biol 14(11):1159–1168. https://doi.org/10.1038/ncb2597
10. Ribeiro SA, Vagnarelli P, Dong Y et al (2010) A super-resolution map of the vertebrate kinetochore. PNAS 107(23):10484–10489. https://doi.org/10.1073/pnas.1002325107
11. Pereira A, Sousa M, Almeida AC et al (2019) Coherent-hybrid STED: high contrast sub-diffraction imaging using a bi-vortex depletion beam. Opt Express 27(6):8092–8111. https://doi.org/10.1364/OE.27.008092
12. Novak M, Polak B, Simunić J et al (2018) The mitotic spindle is chiral due to torques within microtubule bundles. Nat Commun 9:3571. https://doi.org/10.1038/s41467-018-06005-7
13. Vukušić K, Ponjavić I, Buđa R et al (2021) Microtubule-sliding modules based on kinesins EG5 and PRC1-dependent KIF4A drive human spindle elongation. Dev Cell 56(9):1253–1267.e10. https://doi.org/10.1016/j.devcel.2021.04.005
14. Matković J, Ghosh S, Ćosić M et al (2022) Kinetochore- and chromosome-driven transition of microtubules into bundles promotes spindle assembly. Nat Commun 13(1):7307. https://doi.org/10.1038/s41467-022-34957-4
15. Almeida AC, Soares-de-Oliveira J, Drpic D et al (2022) Augmin-dependent microtubule self-organization drives kinetochore fiber maturation in mammals. Cell Rep 39(1):110610. https://doi.org/10.1016/j.celrep.2022.110610
16. Štimac V, Koprivec I, Manenica M et al (2022) Augmin prevents merotelic attachments by promoting proper arrangement of bridging and kinetochore fibers. eLife 11:e83287. https://doi.org/10.7554/eLife.83287
17. Almeida AC, Soares-de-Oliveira J, Maiato H (2023) Optimized protocol for live-cell analysis of kinetochore fiber maturation in Indian muntjac cells. STAR Protoc 4(1):102011. https://doi.org/10.1016/j.xpro.2022.102011
18. Zekušić M, Bujić Mihica M, Skoko M et al (2023) New characterization and safety evaluation of human limbal stem cells used in clinical application: fidelity of mitotic process and mitotic spindle morphologies. Stem Cell Res Ther 14(1):368. https://doi.org/10.1186/s13287-023-03586-z
19. Zeeshan M, Rea E, Abel S et al (2023) Plasmodium ARK2 and EB1 drive unconventional spindle dynamics, during chromosome segregation in sexual transmission stages. Nat Commun 14(1):5652. https://doi.org/10.1038/s41467-023-41395-3
20. Ponjavić I, Vukušić K, Tolić IM (2021) Expansion microscopy of the mitotic spindle. Methods Cell Biol 161:247–274. https://doi.org/10.1016/bs.mcb.2020.04.014
21. Zhang C, Kang JS, Asano SM et al (2020) Expansion microscopy for beginners: visualizing microtubules in expanded cultured HeLa

cells. Curr Protoc Neurosci 92:e96. https://doi.org/10.1002/cpns.96

22. Wong YL, Anzola JV, Davis RL et al (2015) Reversible centriole depletion with an inhibitor of Polo-like kinase 4. Science 348(6239): 1155–1160. https://doi.org/10.1126/science.aaa5111
23. Chen RH, Shevchenko A, Mann M et al (1998) Spindle checkpoint protein Xmad1 recruits Xmad2 to unattached kinetochores. J Cell Biol 143(2):283–295. https://doi.org/10.1083/jcb.143.2.283
24. Magidson V, Paul R, Yang N et al (2015) Adaptive changes in the kinetochore architecture facilitate proper spindle assembly. Nat Cell Biol 17(9):1134–1144. https://doi.org/10.1038/ncb3223
25. Gregan J, Polakova S, Zhang L et al (2011) Merotelic kinetochore attachment: causes and effects. Trends Cell Biol 21(6):374–381. https://doi.org/10.1016/j.tcb.2011.01.003
26. McDonald KL, O'Toole ET, Mastronarde DN et al (1992) Kinetochore microtubules in PTK cells. J Cell Biol 118:369–383. https://doi.org/10.1083/jcb.118.2.369
27. Mastronarde DN, McDonald KL, Ding R et al (1993) Interpolar spindle microtubules in PTK cells. J Cell Biol 123(6):1475–1489. https://doi.org/10.1083/jcb.123.6.1475
28. Sikirzhytski V, Renda F, Tikhonenko I et al (2018) Microtubules assemble near most kinetochores during early prometaphase in human cells. J Cell Biol 217(8):2647–2659. https://doi.org/10.1083/jcb.201710094
29. O'Toole E, Morphew M, McIntosh JR (2020) Electron tomography reveals aspects of spindle structure important for mechanical stability at metaphase. Mol Biol Cell 31(3):184–195. https://doi.org/10.1091/mbc.E19-07-0405
30. Kiewisz R, Fabig G, Conway W et al (2022) Three-dimensional structure of kinetochore-fibers in human mitotic spindles. elife 11: e75459. https://doi.org/10.7554/eLife.75459
31. Merdes A, Stelzer EHK, De Mey J (1991) The three-dimensional architecture of the mitotic spindle, analyzed by confocal fluorescence and electron microscopy. J Electron Microsc Tech 18:61–73. https://doi.org/10.1002/jemt.1060180110
32. McIntosh JR (2001) Electron microscopy of cells: a new beginning for a new century. J Cell Biol 153(6):F25–F32. https://doi.org/10.1083/jcb.153.6.f25
33. Brinkley BR, Cartwright J (1975) Cold labile and cold stable microtubules in the mitotic spindle of mammalian cells. Ann N Y Acad Sci 253:428–439. https://doi.org/10.1111/j.1749-6632.1975.tb19218.x
34. Cai S, O'Connell CB, Khodjakov A et al (2009) Chromosome congression in the absence of kinetochore fibres. Nat Cell Biol 11(7):832–838. https://doi.org/10.1038/ncb1890
35. Kajtez J, Solomatina A, Novak M et al (2016) Overlap microtubules link sister k-fibres and balance the forces on bi-oriented kinetochores. Nat Commun 7:10298. https://doi.org/10.1038/ncomms10298
36. Salmon ED, Cimini D, Cameron LA et al (2005) Merotelic kinetochores in mammalian tissue cells. Philos Trans R Soc Lond Ser B Biol Sci 360(1455):553–568. https://doi.org/10.1098/rstb.2004.1610
37. Etemad B, Kuijt T, Kops G (2015) Kinetochore–microtubule attachment is sufficient to satisfy the human spindle assembly checkpoint. Nat Commun 6:8987. https://doi.org/10.1038/ncomms9987
38. Kuhn J, Dumont S (2017) Spindle assembly checkpoint satisfaction occurs via end-on but not lateral attachments under tension. J Cell Biol 216(6):1533–1542. https://doi.org/10.1083/jcb.201611104
39. Etemad B, Vertesy A, Kuijt TEF et al (2019) Spindle checkpoint silencing at kinetochores with submaximal microtubule occupancy. J Cell Sci 132(12):jcs231589. https://doi.org/10.1242/jcs.231589
40. Cimini D, Moree B, Canman JC et al (2003) Merotelic kinetochore orientation occurs frequently during early mitosis in mammalian tissue cells and error correction is achieved by two different mechanisms. J Cell Sci 116:4213–4225. https://doi.org/10.1242/jcs.00716
41. Sen O, Harrison JU, Burroughs NJ et al (2021) Kinetochore life histories reveal an Aurora-B-dependent error correction mechanism in anaphase. Dev Cell 56(22): 3082–3099.e5. https://doi.org/10.1016/j.devcel.2021.10.007
42. Lukinavičius G, Reymond L, D'Este E et al (2014) Fluorogenic probes for live-cell imaging of the cytoskeleton. Nat Methods 11(7): 731–733. https://doi.org/10.1038/nmeth.2972